Archive of Applied Mechanics (2021) 91:4163–4177
https://doi.org/10.1007/s00419-021-01998-y

ORIGINAL

A. R. Shamshiri · F. Haji Aboutalebi · M. Poursina

A new numerical approach for determination of the Lemaitre's ductile damage parameter in bulk metal forming processes

Received: 14 December 2020 / Accepted: 31 May 2021 / Published online: 12 June 2021

Abstract The damage of materials is the progressive or unexpected deterioration of mechanical strength because of loadings, thermal or chemical effects. The micromechanical damage process of ductile materials is generally studied by the continuum damage mechanics (CDM). One of the most well-known damage models is the Lemaitre's ductile damage criterion. This model only requires one material-dependent parameter to represent damage evolution. In this investigation first, a novel numerical approach is proposed to determine the Lemaitre's ductile damage parameter. Then, a user-defined material subroutine founded on the Lemaitre's ductile damage model is developed. Following, numerical results are achieved for a standard round tensile test specimen. Finally, to validate the suggested method, experimental tests are carried out and compared with the numerical results. The comparison reveals a good agreement and excellent correlation between the numerical and practical results. Hence, it is concluded that the offered numerical approach can accurately determine the Lemaitre's ductile damage parameter as well as the damage behavior of ductile metals.

Keywords New numerical approach · Lemaitre's ductile damage parameter · Bulk metal forming processes · Continuum damage mechanics (CDM)

Abbreviations

A	Total cross section area of RVE
A_D	Damaged area of RVE
D	Damage variable
D_{1C}	Critical damage parameter in tension
e_u	Elongation
E	Young's modulus
$\tilde{E}$	Effective elasticity modulus
f	Yield surface function
G	Shear modulus
I	Second-order identity tensor
K	Hardening coefficient
K	Bulk modulus
n	Hardening power
p	Hydrostatic stress
r	Lemaitre's ductile damage parameter
R	Isotropic hardening function

A. R. Shamshiri · F. Haji Aboutalebi (✉) · M. Poursina
Department of Mechanical Engineering, University of Isfahan, 81746-73441 Isfahan, Iran
e-mail: f.hajiaboutalebi@eng.ui.ac.ir

s Lemaitre's damage power parameter
$\boldsymbol{S}$ Deviatoric stress tensor
ν Poisson's ratio
Y Damage strain energy release rate
$\boldsymbol{\varepsilon}$ Strain tensor
$\boldsymbol{\varepsilon}^d$ Deviatoric strain tensor
$\boldsymbol{\varepsilon}^e$ Elastic strain tensor
ε^p Plastic strain
$\boldsymbol{\varepsilon}^p$ Plastic strain tensor
ε^v Volumetric strain
ε^p_{eq} Equivalent plastic strain
ε_{pd} Threshold plastic strain
$\dot{\boldsymbol{\varepsilon}}^p$ Plastic strain rate tensor
$\dot{\gamma}$ Plastic consistency parameter
η Stress triaxiality
ρ Density
$\boldsymbol{\sigma}$ Stress tensor of virgin material
$\widetilde{\boldsymbol{\sigma}}$ Effective stress tensor
σ_{eq} Von Mises equivalent stress
σ_f Fracture stress
σ_u Ultimate stress
σ^0_y Initial yield stress
ψ Potential dissipation function
ψ_D Damage component of potential dissipation function
ψ_P Plastic component of potential dissipation function

1 Introduction

During various types of loading like plastic deformations, chemical, and thermal, mechanical properties degrade due to damage accumulation and growth that most often leads to failure. This progressive physical process is observed in a wide range of materials such as ductile, brittle, composite, ceramic, concrete, and wood. In ductile materials, the load increasing stops dislocations by microstress concentration. Therefore, it results in nucleation, coalescence, growth, and propagation of microvoids or microcracks usually called ductile damage [1]. Employing a measurable damage variable that denotes material deterioration is highly valuable. The damage variable increases through plastic forming processes and reaches a critical value near macroscopic cracks. In the continuum damage mechanics (CDM), modeling a representative volume element (RVE) at the mesoscale level, damage evolution is taken into account. Therefore, the onset of rupture can be detected.

Applying the concept of one-dimensional surface damage, Kachanov primarily established material damage variable and studied rupture time in a single creep test [2]. Then, the effective stress concept was introduced by Rabotnov to add the damage variable into the constitutive equations as an internal variable [3]. Utilizing the strain equivalence principle, Lemaitre inferred that substituting the effective stress for the usual stress in any strain constitutive equation of undamaged material, the strain constitutive equation is similarly derived for the damaged material [1].

In the last decades, the study of ductile damage behavior and predicting the maximum formability of ductile metals has enabled design engineers to postpone fracture and produce safe parts. A large number of researchers have proposed damage criteria and also modeled the damage behavior of ductile materials. Based on the growth of cylindrical voids, McClintock stated a new ductile damage model to clarify the ductile fracture of materials [4]. Cockcroft and Latham examined the accumulated plastic strain in ductile materials to investigate ductility and the workability of metals [5]. Rice and Tracey conducted a capable model for the enlargement of spherical voids in stress triaxiality fields [6]. Gurson applied the continuum theory of ductile rupture conjugated with void nucleation and growth to predict local damage in uniaxial and biaxial tests [7]. The concept of effective plastic strain and the cumulative strain damage model was tried by Wilkins et al. for ductile fracture of materials [8]. Tvergaard focused on localization in ductile materials with spherical voids [9] and ductile fracture by cavity nucleation effect between larger voids [10]. Moreover, Needleman and Tvergaard developed the origin Gurson's model and founded the famous Gurson–Tvergaard–Needleman (GTN) criterion

[11]. The GTN damage model could successfully follow the damage of materials. However, an expensive machine test was needed to identify the many material-dependent damage parameters by measuring voids evolution at necking and instability zones. Chaboche noticed the damage modeling for anisotropic creep test in the CDM framework [12]. Furthermore, a new and efficient ductile damage criterion combined with the concept of the equivalent strain principle and thermodynamics laws was formulated by Lemaitre [13].

On the other hand, Johnson and Cook extended a damage criterion including the stress triaxiality, plastic strain rate, and temperature terms [14]. Their model relied on five material-dependent damage parameters to estimate damage initiation and evolution in high strain rate deformations. Regarding the irreversible thermodynamics process, Benallal et al. provided an integration algorithm for the fully coupled elastoplastic damage equations [15]. Besides, Steinmann et al. compared various finite deformation inelastic damage models inside the multiplicative elastoplasticity framework for ductile materials [16]. Doghri numerically implemented several metal plasticity models in conjunction with ductile damage [17]. Dhar et al. expressed a CDM model for void growth and microcracks initiation [18]. Referring to the finite strains with linearization aspects, an efficient computational algorithm for the fully coupled elastoplastic damage model was derived by De Souza Neto and Peric [19]. La Rosa et al. obtained a significant correlation between the stress triaxiality factor and logarithmic plastic strain by several CDM models [20].

In the recent century, upgrading the computers and numerical methods such as the finite element method (FEM), extensive researches were quickly performed in the CDM framework. In the absence of kinematic hardening, De Souza Neto simplified the general form of Lemaitre's ductile damage model consisting of 14 nonlinear coupled equations to only one nonlinear scalar equation [21]. Using the irreversible thermodynamics, Brünig offered an anisotropic ductile damage model by the stress triaxiality and the Lode angle parameter effect [22]. Hooputra et al. constructed a comprehensive ductile damage criterion to simulate crashworthiness failure of extruded aluminum parts [23]. A nonlinear damage model in terms of multiaxial stress state was suggested by Bonora et al. [24] for ductile metals. Bai and Wierzbicki assessed a new 3D asymmetric fracture locus with six calibration parameters in the space of the equivalent fracture strain, stress triaxiality, and Lode angle parameter [25]. Based on difference minimization of analytical static and measured displacements, new 2D and 3D algorithms were invented by Rezaiee-Pajand et al. [26]. Zhai et al. paid attention to the damage and dynamic response of reticulated dome subjected to blast loading [27]. Mehditabar and Rahimi considered the cyclic response of functionally graded pipes under thermo-mechanical loads by Chaboche's continuum damage model [28].

It should be emphasized that the above-mentioned damage models depend on a few material-dependent damage parameters, which are determined by a series of experimental tests. The Lemaitre's ductile damage model is known as a simple efficient criterion for accurate predicting of ductile damage and just requires one material-dependent damage parameter. The Lemaitre's ductile damage parameter is generally extracted from practical tests like variations of the elasticity modulus and microhardness methods. In the present study, the main objective is to propose a quick and easy approach for numerical determination of the Lemaitre's ductile damage parameter. Compared with the conventional experimental tests, the current method is simpler, cheaper, and less time-consuming.

2 The standard Lemaitre's ductile damage model

At the microscale level, load increasing leads to breakage of atomic bonds and plastic growth of microcavities, consequently the creation of discontinuities and the onset of damage. At the mesoscale level, the stiffness degradation can be evaluated by an internal variable called damage. This dimensionless variable is simply defined by the ratio of the area of defects to the nominal area of RVE. Assuming the homogeneous distribution of microcavities, the damage variable D is given for a simple one-dimensional loading situation as:

$$D = \frac{\mathrm{A}_D}{\mathrm{A}} \tag{1}$$

$\mathrm{A_D}$ and A, respectively, are the damaged area and total cross section area of the RVE. Therefore, the scalar damage variable D is limited between 0 for undamaged or virgin material and 1 for fractured or fully broken material.

Replacing the stress tensor $\boldsymbol{\sigma}$ with the effective one in any constitutive equation of virgin material, the constitutive equation for damaged material can be easily attained [13]. The effective stress tensor $\widetilde{\boldsymbol{\sigma}}$ is represented by:

$$\widetilde{\boldsymbol{\sigma}} = \frac{\boldsymbol{\sigma}}{1-D} \tag{2}$$

In the absence of reverse loading, the kinematic hardening effect can be ignored in the standard Lemaitre's ductile damage model and only the isotropic hardening effect is mainly noticed. The potential dissipation ψ describes the evolution of internal variables as a scalar convex function of the state variables and is decomposed into the plastic ψ_P and damage ψ_D components:

$$\psi = \psi_P + \psi_D = f + \frac{r}{(1-D)(s+1)}\left(\frac{-Y}{r}\right)^{s+1} \tag{3}$$

where r and s are the Lemaitre's ductile damage material-dependent parameters. Regarding the published experimental results of Lemaitre [13], the parameter s is equal to 1 for ductile metals. f and Y correspondingly are the yield surface function and the damage strain energy release rate:

$$f\left(\boldsymbol{\sigma}, \varepsilon_{eq}^{p}, D\right) = \frac{\sigma_{eq}}{(1-D)} - \left[\sigma_y^0 + R\left(\varepsilon_{eq}^{p}\right)\right] = 0 \tag{4}$$

$$-Y = \frac{\sigma_{eq}^2}{2E(1-D)^2}\left[\frac{2}{3}(1+\upsilon) + 3(1-2\upsilon)\eta^2\right] \tag{5}$$

$$\eta = \frac{p}{\sigma_{eq}} \tag{6}$$

where σ_{eq} is the von Mises equivalent stress, σ_y^0 is the initial yield stress, R is the radial growth of the yield surface (isotropic hardening function), and $\varepsilon_{\mathrm{eq}}^{p}$ is the equivalent plastic strain. Meanwhile, E, υ, η, and p, respectively, are Young's modulus of virgin material, Poisson's ratio, stress triaxiality ratio, and hydrostatic stress. The plastic strain rate tensor $\dot{\boldsymbol{\varepsilon}}^{P}$ is expressed in terms of the deviatoric stress tensor $\boldsymbol{S}$ by the hypothesis of generalized normality:

$$\dot{\boldsymbol{\varepsilon}}^{P} = \dot{\gamma}\frac{\partial \psi}{\partial \boldsymbol{\sigma}} = \dot{\gamma}\sqrt{\frac{3}{2}}\frac{\boldsymbol{s}}{\|\boldsymbol{s}\|} = \frac{3}{2}\dot{\gamma}\frac{\boldsymbol{s}}{\sigma_{eq}} \tag{7}$$

Additionally, the evolution laws for the internal variables are derived as [1]:

$$\dot{\varepsilon}_{eq}^{p} = -\dot{\gamma}\frac{\partial \psi}{\partial R} = \dot{\gamma} \tag{8}$$

$$\dot{D} = -\dot{\gamma}\frac{\partial \psi}{\partial Y} = \dot{\gamma}\frac{1}{1-D}\left(\frac{-Y}{r}\right)^{s} \tag{9}$$

$\dot{\gamma}$ is the plastic consistency parameter in the so-called Kuhn–Tucker loading/unloading conditions:

$$\dot{\gamma} \geq 0,\ f \leq 0,\ \dot{\gamma} f = 0 \tag{10}$$

Based on the standard elastic predictor/plastic corrector (return mapping) algorithm, earlier introduced by Simo and Hughes [29], De Souza Neto simplified the Lemaitre's ductile damage model to only one scalar nonlinear equation. In this efficient algorithm, a typical Gauss point of the finite element mesh within a time interval $[t_n, t_{n+1}]$ with the known values of $\boldsymbol{\sigma}_n, \boldsymbol{\varepsilon}_n^{p}, \varepsilon_{eq,n}^{p}, D_n$ at time t_n is selected. By numerically solving the constitutive equations, the unknown values of $\boldsymbol{\sigma}_{n+1}, \boldsymbol{\varepsilon}_{n+1}^{p}, \varepsilon_{eq,n+1}^{p}, D_{n+1}$ are calculated at the end of the interval, time t_{n+1}. The complete details of the fully coupled elastoplastic damage integration algorithm are available in [21], which are explicitly summarized in Table 1.

Table 1 Elastic predictor/plastic corrector (return mapping) algorithm [21]

Step 1- Elastic predictor: for a given strain increment of $\Delta\boldsymbol{\varepsilon}$ and the state of variables at the time t_n , compute:

$$\boldsymbol{\varepsilon}_{n+1}^{e,trial} = \boldsymbol{\varepsilon}_n^e + \Delta\boldsymbol{\varepsilon} \quad , \quad \varepsilon_{eq,n+1}^{p,trial} = \varepsilon_{eq,n}^p \quad , \quad D_{n+1} = D_n$$

$$\boldsymbol{s}^{trial} = \boldsymbol{s}_n + 2\mathrm{G}\,\Delta\boldsymbol{\varepsilon}^d \quad , \quad p^{trial} = p_n + \mathrm{K}\,\Delta\varepsilon^{\mathrm{v}}$$

Step 2- Check the plastic consistency conditions:

$$f^{trial} = \sqrt{\frac{3}{2}}\frac{\|\boldsymbol{s}^{trial}\|}{(1-D_n)} - \left[\sigma_y^0 + R\left(\varepsilon_{eq,n}^p\right)\right]$$

if $f^{trial} \le 0$ then Elastic step: update $(\#)_{n+1} = (\#)^{trial}$

$$\boldsymbol{\sigma}_{n+1} = \boldsymbol{s}_{n+1} + p_{n+1}\,\mathbf{I}$$

Return to step 1

Else Plastic step, return mapping algorithm:

Step 3- Solve for Δγ:

$$D(\Delta\gamma) - D_n - \frac{\Delta\gamma}{1-D(\Delta\gamma)}\left(\frac{-Y(\Delta\gamma)}{r}\right)^s = 0$$

$$D(\Delta\gamma) = D_{n+1} = 1 - \frac{\sqrt{\frac{3}{2}}\left\|\mathbf{s}^{trial}\right\| - 3\mathrm{G}\Delta\gamma}{\sigma_y^0 + R\left(\varepsilon_{eq,n}^p + \Delta\gamma\right)}$$

Step 4- Update variables:

$$\boldsymbol{s}_{n+1} = \left(1 - \sqrt{\frac{3}{2}}\frac{2\mathrm{G}\Delta\gamma}{\|\boldsymbol{s}^{trial}\|}\right)\boldsymbol{s}^{trial} \quad , \quad p_{n+1} = p^{trial} \quad , \quad \varepsilon_{eq,n+1}^p = \varepsilon_{eq,n}^p + \Delta\gamma \quad , \quad D_{n+1} = D(\Delta\gamma)$$

$$\boldsymbol{\sigma}_{n+1} = \boldsymbol{s}_{n+1} + p_{n+1}\,\mathbf{I} \quad , \quad \boldsymbol{\varepsilon}_{n+1}^e = \frac{1}{2\mathrm{G}}\boldsymbol{S}_{n+1} + \frac{1}{3\mathrm{K}}\,p_{n+1}\,\mathbf{I}$$

End if

Return to step 1

3 New proposed method

In this section, a novel numerical approach is presented to determine the Lemaitre's ductile damage parameter r only from one standard simple tensile test results. The suggested approach is easier, cheaper, and faster than the experimental methods, such as variations of the elasticity modulus and microhardness tests. For numerical determination of the Lemaitre's ductile damage parameter for a desired ductile metal, the following steps are offered:

Step 1 A standard bulk specimen is prepared and empirically drawn until fracture by a uniaxial tensile test machine.

Step 2 The conventional mechanical properties of the material consisting of the Young's modulus, yield stress, and isotropic hardening coefficients are achieved via the provided engineering and true stress–strain diagrams.

Step 3 An initial guess value is chosen for the damage parameter r. This value is generally between 0.5 and 12 Mpa, regarding the former practical researches for ductile metals [30–33].

Step 4 The standard tensile test is numerically simulated through a finite element model, established in Table 1. After the finite element simulations, the force–displacement and engineering stress–strain diagrams are numerically obtained and compared with the empirical curves.

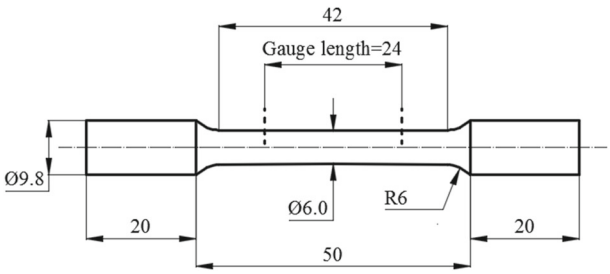

Fig. 1 Geometry of the standard round tensile test specimen (all dimensions are in mm)

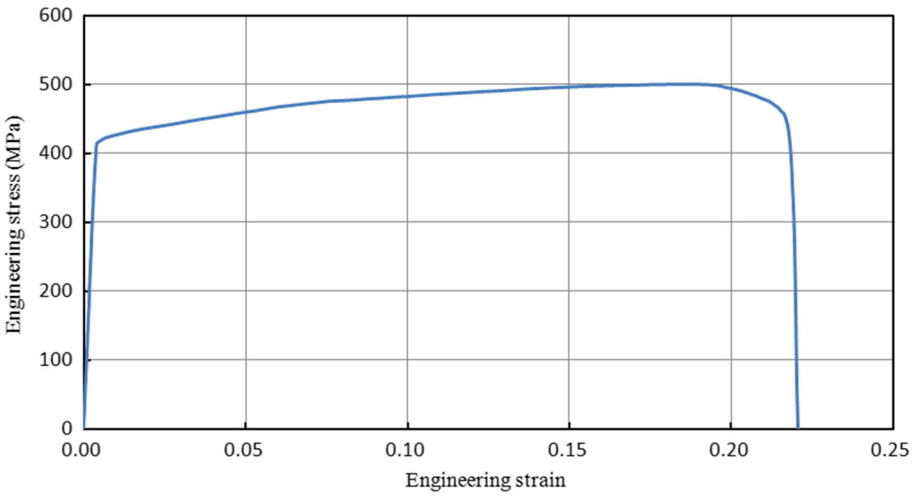

Fig. 2 Engineering stress–strain curve for the annealed 16MnCr5 steel

Step 5 If the numerical and experimental diagrams are in good accordance and show adequate correlation, the initial trial value is accepted as the true value for the Lemaitre's ductile damage parameter *r*.

Step 6 Else, a new guess value is tried and step 4 is repeated until the comparison of numerical and practical results exhibits sufficient adaptation. After reaching a proper agreement between the numerical and empirical results, the last trial value is finalized for the Lemaitre's ductile damage parameter *r*.

The proposed approach may not accurately predict pure shear or pure torsion loadings, due to ignoring the effect of the Lode angle parameter addressed by Bai and Wierzbicki [25] and Cao et al. [34]. Moreover, regarding Papasidero et al. [35] and Gerke et al. [36], using the damage and fracture models with non-proportional loading histories can lead to more accurate results for large deformation processes. Additionally, the anisotropic plasticity and anisotropic damage models conducted by Autay et al. [37] and Ghorbel et al. [38, 39] are highly recommended for anisotropic metals.

4 Mechanical properties

Referring to the Euro standard classification "EN 10084:1998" [40], the DIN 1.7131 steel, so-called 16MnCr5 steel, was selected. The material is extensively applied in industrial parts such as gears, shafts, camshafts, and gudgeon pins which need high strength and durability. As demonstrated in Fig. 1, the required round tensile test specimens were prepared by CNC machining according to the E8/E8M-16a standard [41].

The samples were annealed to remove the probable residual stresses of the machining operations. A SANTAM multipurpose testing machine with a max capacity of 20 KN was employed to draw the instances at the fixed rate of 0.5 mm/min and room temperature until fracture. For reliability and accuracy, the practical tensile test was repeated three times and the results were averaged. Figure 2 illustrates the averaged results of the engineering stress–strain curve for the annealed round tensile test specimen in the uniaxial tensile test.

As Fig. 3 clarifies, Ludwick's power law is utilized to express the plastic behavior and isotropic hardening of the annealed material by a simple curve-fitting on the true plastic stress–strain diagram. Comparison of the

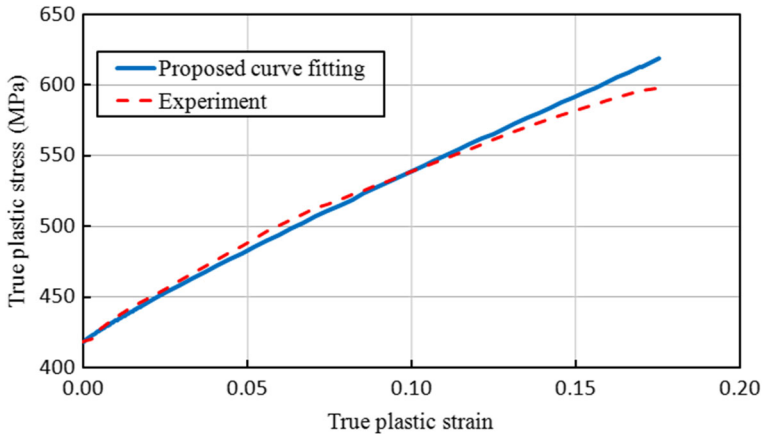

Fig. 3 True plastic stress–strain and proposed curve-fitting for the annealed 16MnCr5 steel

Table 2 Mechanical properties of the annealed 16MnCr5 steel

Parameter	Value	Standard deviation
Young's modulus, E(GPa)	210	2.16
Initial yield stress,σ_y^0(MPa)	418	5.89
Ultimate stress,σ_u(MPa)	505	1.70
Fracture stress,σ_f (MPa)	282	6.68
Elongation, e_u(%)	22.08	0.10
Hardening coefficient, K(MPa)	956.81	7.31
Hardening power, n	0.8984	0.01

Table 3 Mesh study results for the center point of the sample at a displacement of 5.478 mm

Element size (mm)	Damage variable	Percentage of changes
1.0	0.2950	–
0.5	0.3611	22.40
0.4	0.4068	12.65
0.3	0.4348	6.88
0.25	0.4386	0.87

experimental and the fitted curves shows a maximum error percentage of 3.3% and a correlation coefficient of + 0.9976, which is reasonable and satisfactory. Table 2 lists the mean values and standard deviation of mechanical properties for the annealed material, extracted from both the engineering and true stress–strain curves.

5 Numerical determination of damage parameter

To examine the novel numerical approach, the standard 16MnCr5 steel sample was numerically simulated. For this aim, a user-defined material subroutine found on the Lemaitre's ductile damage model algorithm (Table 1) was developed and implemented into an explicit code. Referring to the ductile damage modeling in the mesoscale, the proper mesh size for ductile metals is strongly recommended to be between 0.1 and 0.5 mm [1, 13]. To ensure the mesh non-dependence of the numerical results, a mesh study was performed. Table 3 indicates the results for the center point at a displacement of 5.478 mm, where the instance is exposed to great plastic deformation. The results reveal that at the element size of 0.25 mm, the percentage of changes is less than one percent and the damage variable converges. Thus, this element size is fixed for all of the numerical simulations.

As depicted in Fig. 4, a fine mesh with the size of 0.25 mm was assigned to the center zone of the specimen, which is subjected to high magnitudes of the stress triaxiality and faster damage growth. Due to symmetry, only one-eighth of the sample was discretized by a total number of 4704 eight nodes bilinear 3D

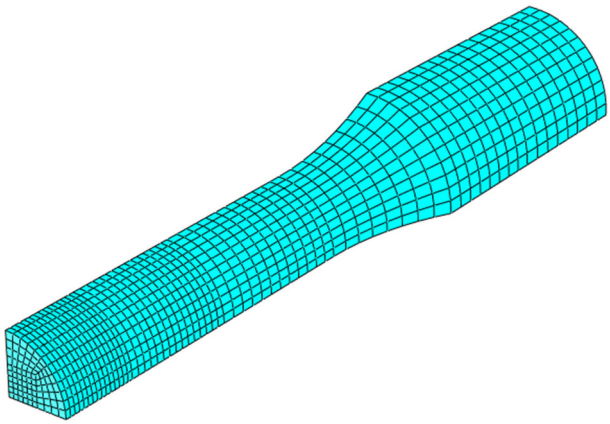

Fig. 4 One-eighth of the finite element model for the standard round tensile test specimen

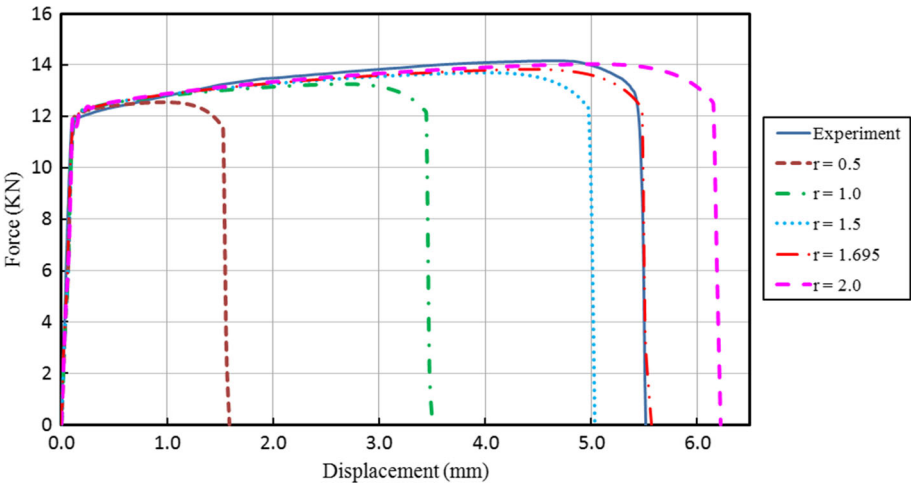

Fig. 5 Numerical determination of the Lemaitre's ductile damage parameter r

stress quadrilateral elements. The symmetry conditions were imposed on the symmetry planes, and the end surface was monotonically drawn.

As explained in Sect. 3, different guess values for the ductile damage parameter r were tried and the damage parameter was numerically determined for the material by the new offered method. Figure 5 displays the comparison of the force–displacement diagrams, predicted by the numerical simulations with different guess values and the experimental results. As clarified, the value of 1.695 MPa closely follows the empirical curve and the failure of the specimen, which occurs at 5.52 mm. The maximum error percentage of 2.58% at the displacement of 4.7 mm and the correlation coefficient of + 0.9932 completely validates the accuracy of the determined value.

The numerical simulations were continued until the value of the damage variable in the elements reached the critical damage parameter D_{1c}. Then, the stresses of critical elements were released, well known as the element deletion technique in the finite element numerical analyses. D_{1c} is a material-dependent damage parameter between 0.2 and 0.5 for all types of steel alloys. However, it is specified by practical tests, and there is an approximate formula to estimate the magnitude of this parameter for ductile metals [1]:

$$D_{1c} = 1 - \frac{\sigma_f}{\sigma_u} \tag{11}$$

where σ_f and σ_u, respectively, are the fracture and ultimate stresses of the material. Referring to Table 2, the critical damage parameter was approximated to be 0.4415, which was used for the element deletion technique.

Figure 6 illustrates the damage evolution results of the specimen at several displacements until complete fracture. Increasing the displacement leads to faster damage growth in the center zone of the instance rather

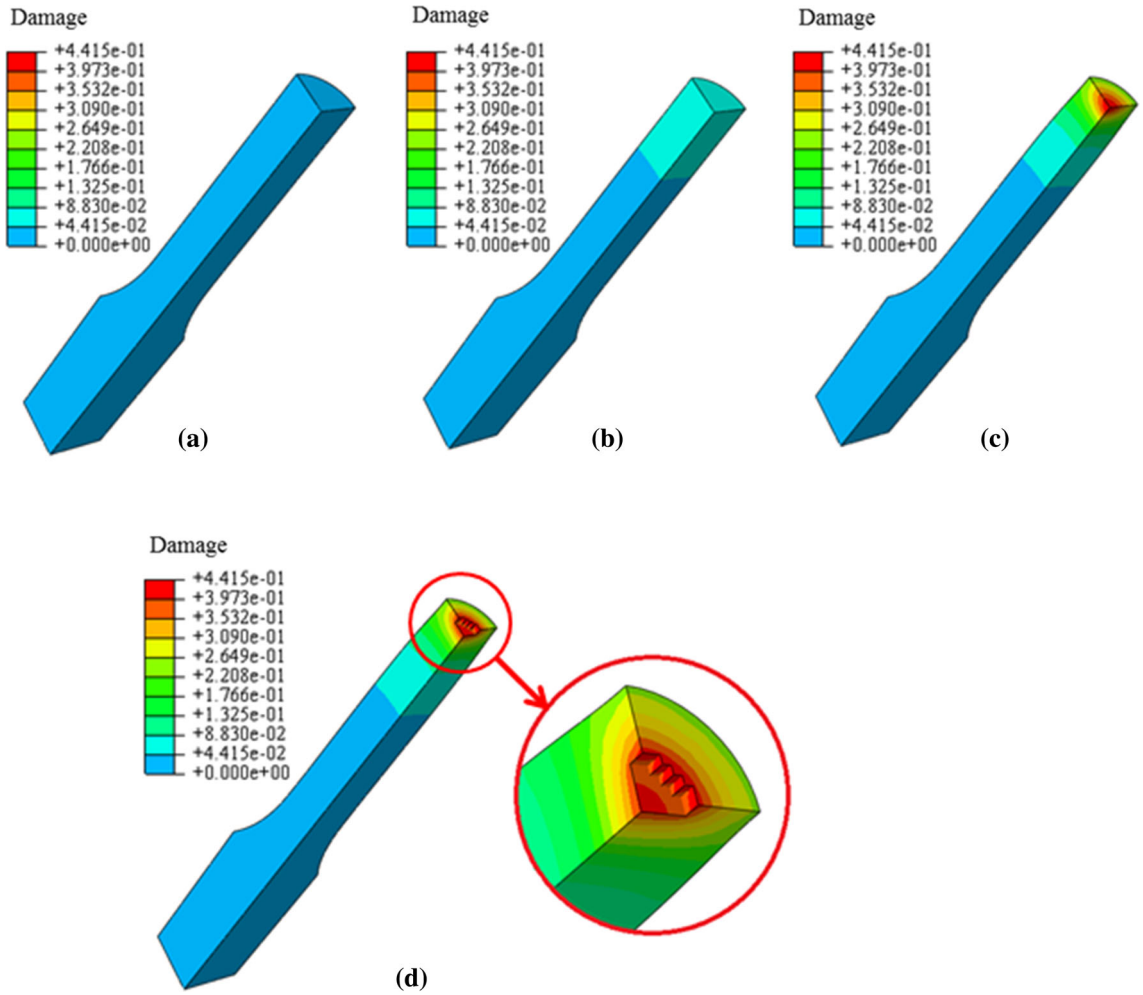

Fig. 6 Damage evolution results for the standard tensile test at displacements of: **a** 2.084 mm, **b** 4.984 mm, **c** 5.478 mm, and **d** 5.488 mm (fracture initiation)

than in other regions. As clearly seen, the ductile damage variable reaches the critical damage parameter value at the final displacement of 5.488 mm, and fracture initiates.

Besides, the history of the stress triaxiality growth vs. the ductile damage variable at three separate points of (a), (b), and (c) located on the central cross section of the instance is compared in Fig. 7. As the figure confirms, the stress triaxiality ratio for the three points has initially constant nominal value of 0.33, which is expected for the uniaxial tensile test. However, the values of stress triaxiality rapidly change, due to the large deformation and non-uniformity of stress distribution in the central section. Growing the stress triaxiality ratio leads to the damage evolution and failure of the part. Rather than others, the stress triaxiality ratio more quickly grows in the central point of (a) with increasing the loading. Moreover, Fig. 8 compares the damage variable versus the equivalent plastic strain at the three different points of (a), (b), and (c). The comparison obviously indicates that the point of (a) earlier touches the critical damage value of 0.4415, during the loading. As previously mentioned, damage growth in ductile metals extremely depends on the two factors of stress triaxiality ratio and the equivalent plastic strain. Therefore, point (a) sooner reaches the critical damage value and fracture starts from this point.

6 Validation

To validate the determined damage parameter and the new approach, the Lemaitre's ductile damage parameter is experimentally achieved and compared with the numerically determined value. Regarding the investigations of

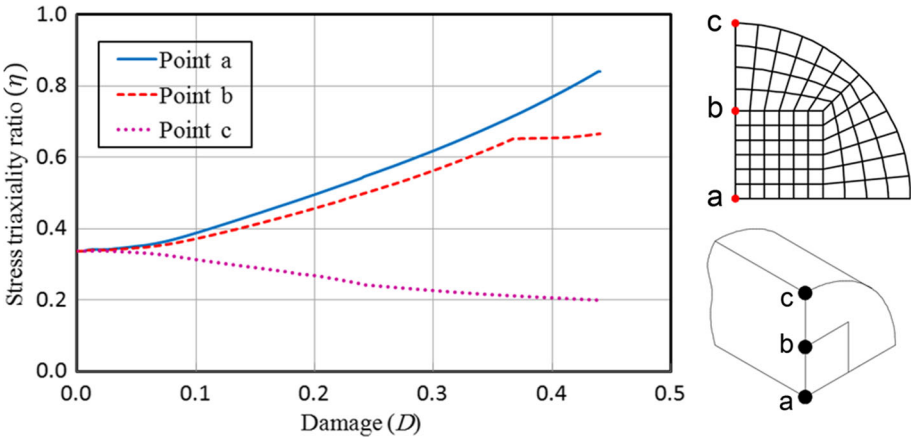

Fig. 7 Stress triaxiality growth versus ductile damage variable for the three different points of (**a**), (**b**), and (**c**) on the central cross section of the sample

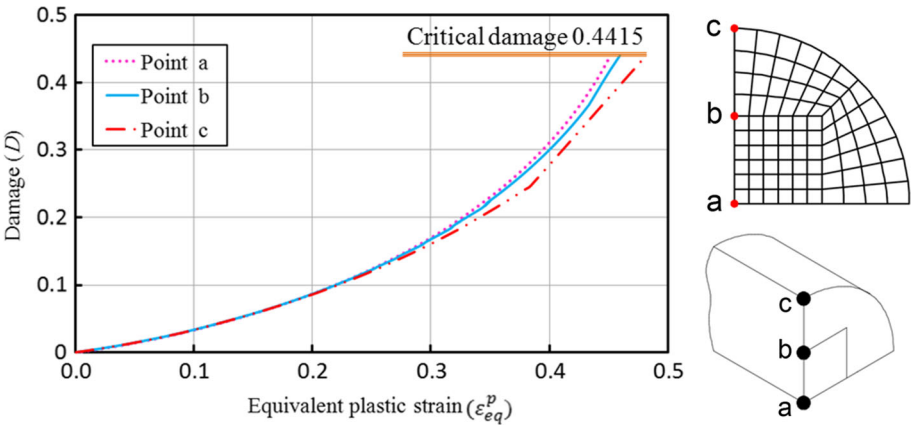

Fig. 8 Comparison of damage variable versus equivalent plastic strain for the three different points of (**a**), (**b**), and (**c**) on the central cross section of the sample

Lemaitre [1, 13], two types of direct and indirect methods exist for measuring the ductile damage parameter of materials. The direct method is a destructive approach which works based on observing micrograph pictures of the material. It accounts for the cross section area of microvoids and damaged zones and requires very accurate and sensitive image processing tools. On the other hand, indirect methods detect variations of a physical or mechanical property in a damaged material. These approaches consist of density, electrical resistance, propagation of ultrasonic waves, tertiary creep response, cyclic plasticity response, elasticity modulus, and microhardness methods. The variations of microhardness and elasticity modulus approaches are the most accurate methods for ductile metals. Haji Aboutalebi et al. applied the Vickers microhardness method and practically obtained the Lemaitre's ductile damage parameter for DIN1623 St14 steel [31]. In the current research, the method of elasticity modulus variations is employed to experimentally specify the Lemaitre's ductile damage parameter for the 16MnCr5 steel.

6.1 Variations of elasticity modulus method

Deterioration of material through a successive loading–unloading tensile test causes to the reduction of the elasticity modulus. Thus, tracking the slopes of unloading lines allows following different stages of damage evolution in the material. For a homogeneous and isotropic material, the isotropic damage can be simply attained as:

$$D = 1 - \frac{\tilde{E}}{E} \tag{12}$$

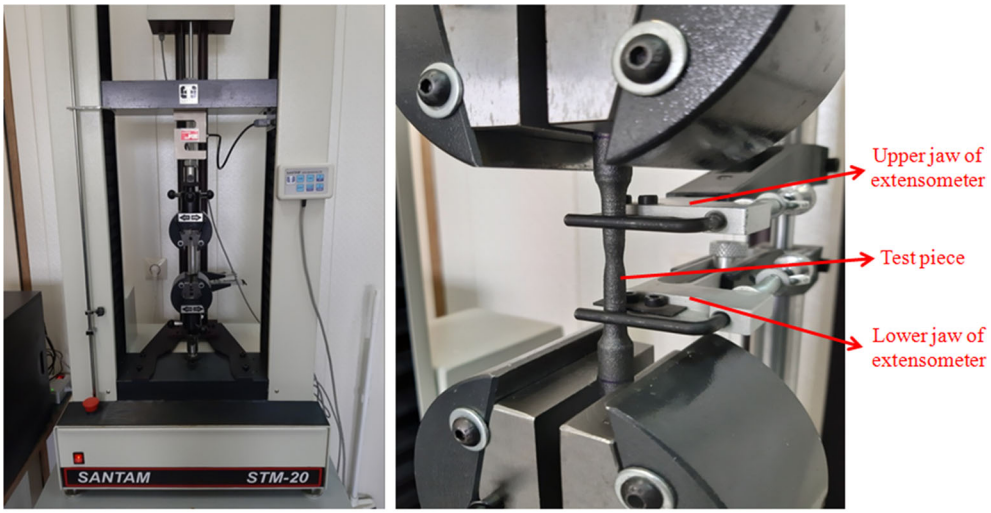

Fig. 9 **a** SANTAM testing machine and (**b**) annealed round tensile test specimen

where E and $\tilde{E}$ correspondingly are Young's modulus of virgin material and effective elasticity modulus of damaged material. The effective elasticity modulus is extracted from the slope of each unloading path in the engineering stress–strain curve. Additionally, the Lemaitre's ductile damage parameter r is given by the below relation [30]:

$$r = \frac{\sigma^2}{2E(1-D)^2(\frac{dD}{d\varepsilon^p})} \tag{13}$$

6.2 Loading–unloading test

According to the previous descriptions of Sect. 4, three new annealed round tensile test specimens were similarly provided. Each instance was individually exposed to the successive loading–unloading conditions, and the results were averaged for reliability and accuracy. As depicted in Fig. 9, an accurate, sensitive extensometer with large gauge length was used for precisely recording the strains.

Referring to Fig. 5, the total fracture displacement can be divided into a number of divisions, which is adjusted as the needed displacement for the start point of each unloading path. In this study, a total number of 16 divisions were fixed to precisely achieve the Lemaitre's ductile damage parameter. After any of the unloading stages, the slope of the unloading tangent line in the engineering stress–strain diagram denotes an effective elasticity modulus of the material, as Fig. 10 exhibits. In comparison with the monotonic loading diagram of Fig. 5, the test specimen fails at more elongation. It is because of the accumulation of the residual stresses in the hysteresis cycles of the loading–unloading.

Having the magnitudes of effective elasticity modulus, the damage variable D can be easily found by Eq. (12) for each step. Figure 11 demonstrates the variations of the damage variable versus the true plastic strain in every of the unloading stages and also the related error bars. For higher accuracy, two different types of linear and polynomial regression were utilized in the curve-fitting process. The figure clearly reveals that a threshold plastic strain of about 0.02985 exists for the damage initiation process. The magnitude of damage variable is highly insignificant for the equivalent plastic strains less than the threshold plastic strain.

Using Fig. 11, the slope of damage variable versus the equivalent plastic strain is calculated, as listed in Table 4. Eventually, the ductile damage parameter r can be attained by Eq. (13) for each of the unloading stages. Regarding Eq. (13), the value of Lemaitre's ductile damage parameter r depends on the magnitudes of stress, damage variable, and slope of the tangent line. Thus, various magnitudes of the mentioned parameters give different values for the damage parameter in every step. Averaging the values of r can lead to the overall prediction of damage growth and damage behavior of material throughout the loading history [1]. Meanwhile, Fig. 12 displays the error bars of the damage parameter for the three empirical tests.

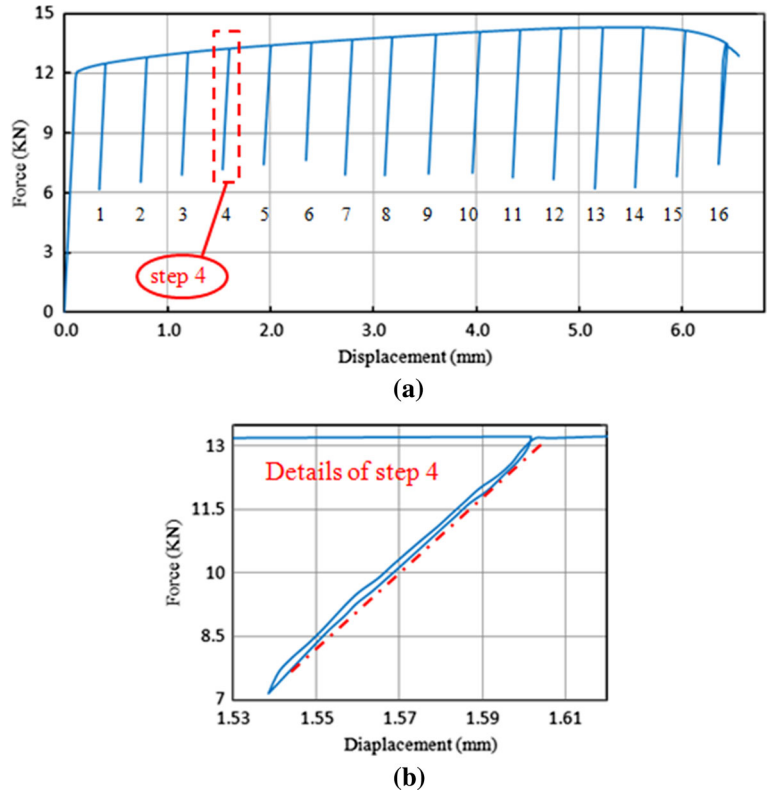

Fig. 10 Results of the experimental successive loading–unloading test: **a** force–displacement curve and (**b**) details of the tangent line to the unloading curve

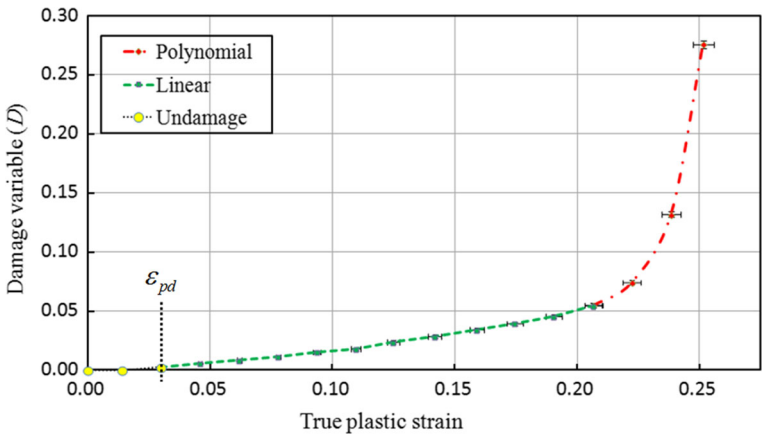

Fig. 11 Variations of damage variable versus true plastic strain and error bars

The mean magnitude of r is computed equal to 1.707 MPa, which represents the intended value of Lemaitre's ductile damage parameter. On the other hand, the damage parameter was numerically determined to be 1.695 MPa by the proposed method in Sect. 5. Comparing the determined and experimental values shows a very low error percentage of 0.7%, which is satisfactory. Therefore, the practical tests strongly confirm that the current novel numerical approach is able to successfully determine the Lemaitre's ductile damage parameter as well as the damage behavior of ductile metals.

Table 4 Experimental loading–unloading test results

Unloading steps	$\tilde{E}$(GPa)	D	The standard deviation of D	r (MPa)	The standard deviation of r
1	210.0	0.00000	0.00	–	–
2	209.5	0.00238	1.46e-4	1.8341	6.55e-3
3	208.8	0.00571	3.67e-4	1.9169	9.60e-3
4	208.2	0.00857	6.59e-4	1.9858	1.36e-2
5	207.6	0.01142	9.55e-4	2.0469	1.85e-2
6	206.8	0.01523	1.10e-3	2.1063	1.88e-2
7	206.2	0.01809	1.32e-3	2.1600	1.61e-2
8	205.0	0.02381	1.43e-3	2.2214	2.18e-2
9	204.0	0.02857	1.44e-3	2.2966	2.63e-2
10	202.8	0.03428	1.51e-3	2.3536	2.32e-2
11	201.7	0.03952	1.65e-3	2.4239	2.58e-2
12	200.4	0.04571	1.84e-3	2.4722	2.34e-2
13	198.5	0.05476	2.04e-3	1.2878	4.90e-2
14	194.4	0.07428	2.17e-3	0.3132	3.22e-2
15	182.3	0.13190	2.50e-3	0.1142	2.48e-2
16	152.1	0.27571	3.00e-3	0.0725	2.00e-2

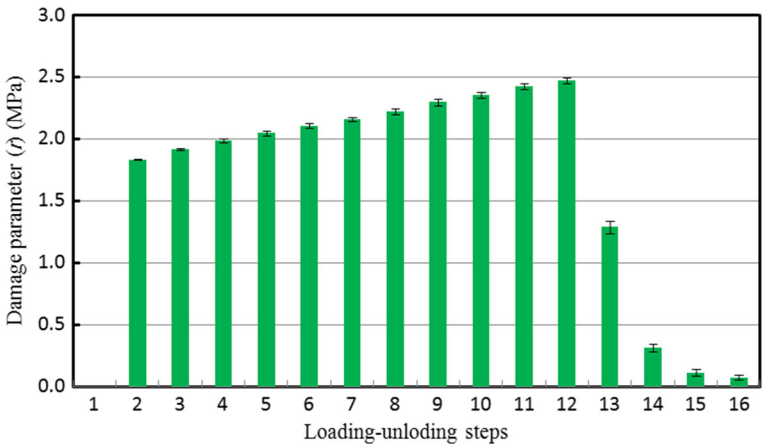

Fig. 12 Error bars diagram for ductile damage parameter r

7 Conclusions

In this paper, the major objective was to propose a new efficient approach for numerically determining the Lemaitre's ductile damage parameter in ductile metals. The suggested method only required the empirical results of one simple uniaxial tensile test for a desired material. Compared with the conventional experimental approaches, the presented approach was much easier, faster, and cheaper. The current method was examined for the so-called 16MnCr5 steel material. The Lemaitre's ductile damage parameter was numerically determined by a user-defined material subroutine. Furthermore, to validate the novel approach, the successive loading–unloading tensile test was conducted to practically obtain the ductile damage parameter. The numerical and empirical values of the ductile damage parameter were compared. The comparison revealed a very insignificant percentage of error and excellent correlation. The offered approach can numerically determine the Lemaitre's ductile damage parameter without any high-cost and time-consuming empirical tests. Hence, it is concluded that the numerically suggested method can be confidently employed for numerically determining the damage behavior of ductile metals in bulk metal forming processes.

Declarations

Conflict of interest On behalf of all authors, the corresponding author states that there is no conflict of interest.

References

1. Lemaitre, J.: A course on damage mechanics. Springer, Cham (2012)
2. Kachanov, L.M.: On the time to failure under creep conditions. Izv. AN SSSR Otd. Tekhn. Nauk. **8**, 26–31 (1958)
3. Rabotnov, Y.N.: A model of an elastic-plastic medium with delayed yield. J. Appl. Mech. Tech. Phys. **9**(3), 265–269 (1968)
4. McClintock, F.A.: A criterion for ductile fracture by the growth of holes. Int. J. Fract. Mech. (1968). https://doi.org/10.1007/BF00188939
5. Cockcroft, M.G., Latham, D.J.: Ductility and the workability of metals. J. Inst. Met. **96**(1), 33–39 (1968)
6. Rice, J.R., Tracey, D.M.: On the ductile enlargement of voids in triaxial stress fields. J. Mech. Phys. Solids **17**(3), 201–217 (1969)
7. Gurson, A.L.: Continuum theory of ductile rupture by void nucleation and growth: part I—Yield criteria and flow rules for porous ductile media. J. Eng. Mater. Technol. **99**(1), 2–15 (1977)
8. Wilkins, M. L., Streit, R. D., & Reaugh, J. E. (1980). Cumulative-strain-damage model of ductile fracture: simulation and prediction of engineering fracture tests (No. UCRL-53058). Lawrence Livermore National Lab., CA (USA); Science Applications, Inc., San Leandro, CA (USA)
9. Tvergaard, V.: On localization in ductile materials containing spherical voids. Int. J. Fract. **18**(4), 237–252 (1982)
10. Tvergaard, V.: Ductile fracture by cavity nucleation between larger voids. J. Mech. Phys. Solids **30**(4), 265–286 (1982)
11. Needleman, A., Tvergaard, V.: An analysis of ductile rupture in notched bars. J. Mech. Phys. Solids **32**(6), 461–490 (1984)
12. Chaboche, J.L.: Anisotropic creep damage in the framework of continuum damage mechanics. Nucl. Eng. Des. **79**(3), 309–319 (1984)
13. Lemaitre, J.: A continuous damage mechanics model for ductile fracture. J. Eng. Mater. Technol. **107**(1), 83–89 (1985)
14. Johnson, G.R., Cook, W.H.: Fracture characteristics of three metals subjected to various strains, strain rates, temperatures and pressures. Eng. Fract. Mech. **21**(1), 31–48 (1985)
15. Benallal, A., Billardon, R., Doghri, I.: An integration algorithm and the corresponding consistent tangent operator for fully coupled elastoplastic and damage equations. Commun. Appl. Numer. Methods **4**(6), 731–740 (1988)
16. Steinmann, P., Miehe, C., Stein, E.: Comparison of different finite deformation inelastic damage models within multiplicative elastoplasticity for ductile materials. Comput. Mech. **13**(6), 458–474 (1994)
17. Doghri, I.: Numerical implementation and analysis of a class of metal plasticity models coupled with ductile damage. Int. J. Numer. Meth. Eng. **38**(20), 3403–3431 (1995)
18. Dhar, S., Sethuraman, R., Dixit, P.M.: A continuum damage mechanics model for void growth and micro crack initiation. Eng. Fract. Mech. **53**(6), 917–928 (1996)
19. De. Souza Neto, E.A., Peric, D.: A computational framework for a class of fully coupled models for elastoplastic damage at finite strains with reference to the linearization aspects. Comput. Methods Appl. Mech. Eng. **130**(1–2), 179–193 (1996)
20. La. Rosa, G., Mirone, G., Risitano, A.: Effect of stress triaxiality corrected plastic flow on ductile damage evolution in the framework of continuum damage mechanics. Eng. Fract. Mech. **68**(4), 417–434 (2001)
21. De. Souza Neto, E.A.: A fast, one-equation integration algorithm for the Lemaitre ductile damage model. Commun. Numer. Methods Eng. **18**(8), 541–554 (2002)
22. Brünig, M.: An anisotropic ductile damage model based on irreversible thermodynamics. Int. J. Plast **19**(10), 1679–1713 (2003)
23. Hooputra, H., Gese, H., Dell, H., Werner, H.: A comprehensive failure model for crashworthiness simulation of aluminium extrusions. Int. J. Crashworthiness **9**(5), 449–464 (2004)
24. Bonora, N., Gentile, D., Pirondi, A., Newaz, G.: Ductile damage evolution under triaxial state of stress: theory and experiments. Int. J. Plast **21**(5), 981–1007 (2005)
25. Bai, Y., Wierzbicki, T.: A new model of metal plasticity and fracture with pressure and lode dependence. Int. J. Plast **24**(6), 1071–1096 (2008)
26. Rezaiee-Pajand, M., Kazemiyan, M.S., Aftabi, S.A.: Static damage identification of 3D and 2D frames. Mech. Based Des. Struct. Mach. **42**(1), 70–96 (2014)
27. Zhai, X., Wang, Y., Sun, Z.: Damage model and damage assessment for single-layer reticulated domes under exterior blast load. Mech. Based Des. Struct. Mach. **47**(3), 319–338 (2019)
28. Mehditabar, A., Rahimi, G.H.: Cyclic elastoplastic responses of thick-walled FG pipe behaves as a power law function considering damage evolution. Mech. Based Des. Struct. Mach. (2020). https://doi.org/10.1080/15397734.2020.1768112
29. Simo, J.C., Hughes, T.J.R.: Interdisciplinary applied mathematics. In: Bloch, A., Epstein, C.L., Goriely, A., Greengard, L. (eds.) Mechanics and materials, computational inelasticity. Springer-Verlag, New York (1998)
30. Mashayekhi, M., Ziaei-Rad, S., Parvizian, J., Niklewicz, J., Hadavinia, H.: Ductile crack growth based on damage criterion: experimental and numerical studies. Mech. Mater. **39**(7), 623–636 (2007)
31. Haji Aboutalebi, F., Farzin, M., Poursina, M.: Numerical simulation and experimental validation of a ductile damage model for DIN 1623 St14 steel. Int. J. Adv. Manuf. Technol. **53**(1–4), 157–165 (2011)
32. Haji Aboutalebi, F., Farzin, M., Mashayekhi, M.: Numerical predictions and experimental validations of ductile damage evolution in sheet metal forming processes. Acta Mech. Solida Sin. **25**(6), 638–650 (2012)
33. Haji Aboutalebi, F., Roostaei, M., Safaie, P.: Empirical determination of Lemaitre's ductile damage parameters for thin sheet metals by variations of the elasticity modulus. Steel Res. Int. **83**(Special Issue), 1195–1198 (2012)
34. Cao, T.S., Gachet, J.M., Montmitonnet, P., Bouchard, P.O.: A Lode-dependent enhanced Lemaitre model for ductile fracture prediction at low stress triaxiality. Eng. Fract. Mech. **124**, 80–96 (2014)
35. Papasidero, J., Doquet, V., Mohr, D.: Ductile fracture of aluminum 2024–T351 under proportional and non-proportional multi-axial loading: Bao-Wierzbicki results revisited. Int. J. Solids Struct. **69**, 459–474 (2015)
36. Gerke, S., Zistl, M., Brünig, M.: Experiments and numerical simulation of damage and fracture of the X0-specimen under non-proportional loading paths. Eng. Fract. Mech. **224**, 106795 (2020)
37. Autay, R., Koubaa, S., Wali, M., Dammak, F.: Numerical implementation of coupled anisotropic plasticity-ductile damage in sheet metal forming process. J. Mech. **34**(4), 417–430 (2018)

38. Ghorbel, O., Koubaa, S., Mars, J., Wali, M., Dammak, F.: Non associated-anisotropic plasticity model fully coupled with isotropic ductile damage for sheet metal forming applications. Int. J. Solids Struct. **166**, 96–111 (2019)
39. Ghorbel, O., Mars, J., Koubaa, S., Wali, M., Dammak, F.: Coupled anisotropic plasticity-ductile damage: modeling, experimental verification, and application to sheet metal forming simulation. Int. J. Mech. Sci. **150**, 548–560 (2019)
40. Bringas, J.E.: Handbook of comparative world steel standards. ASTM, United States (2002)
41. Standard E8/E8M-16a (2016). Standard test methods for tension testing of metallic materials. An American National Standard. AASHTO No.: T68. pp. 8